Investigation of Effect of Fullerenol on Viscoelasticity Properties of human hepatocellular carcinoma by AFM-Based Creep Tests

Xinyao Zhu[a)], Zuobin Wang[b)] and X. Liu[a)*]

[a)] *School of Engineering, University of Warwick, Coventry CV4 7AL, UK*

[b)] *International Research Centre for Nano Handling and Manufacturing of China, Changchun University of Science and Technology, Changchun 130022, China*

Corresponding author: Tel: +44(0)24 765 23136, Fax: +44(0)24 76 418922

Email: X.Liu@warwick.ac.uk

Abstract: Cellular elasticity is frequently measured to investigate the biomechanical effects of drug treatment, diseases and aging. In light of cellular viscosity property exhibited by filament actin networks, this study investigates the viscoelasticity alterations of human hepatocellular carcinoma (SMMC-7721) cell subjected to fullerenol treatment by means of creep tests realized by AFM indentation. An SMMC-7721 cell was first modeled as a sphere and then a flattened layer with finite thickness. Both Sneddon's solutions and Dimitriadis model have been modified to adapt for viscoelastic situation, which are used to fit the same indentation depth – time curves obtained by creep tests. We find that the SMMC-7721 cell's creep behavior is well described by the two modified models, and the divergence of parameters determined by the two models is justified. By fullerenol treatment, the SMMC-7721 cell exhibits a significant decrease of elastic modulus and viscosity, which is presumably due to the disruption of actin filaments. This work represents a new attempt to understand the alternation of the viscoelastic properties of cancerous cells under the treatment of fullerenol, which has the significance of comprehensively elucidating the biomechanical effects of anticancer agents (such as fullerenol) on cancer cells.

I. INTRODUCTION

Since the discovery of buckminsterfullerene (C_{60}) in 1985, fullerenes have been attracting much attention for its potential function in biomedical areas, e.g. cancer diagnosis and therapy.[1] Despite of its promising medical prospects, C_{60} has inferior solubility in aqueous solutions which prevents its popularity in biological applications.[2] However, this issue is circumvented to a great extent by chemical or supramolecular method, and thus various functionalized fullerenes have been compounded to achieve promising results.[3] For example, by adding hydroxyl groups onto fullerene molecules, a fullerene derivative termed as fullerenol [$C_{60}(OH)_n$], is synthesized which exhibits good water solubility and biological compatibility.[4, 5]

Recent work has shown that fullerenol could impact the cytoskeletal structure whose dynamic alterations are correlated with physiological and pathological processes, e.g. cell growth, differentiation, cancer proliferation, metastasis and apoptosis. Zhou et al.[6] indicated that the disruption of the actin cytoskeleton and microtubule network can induce apoptotic events. Johnson-Lyles et al.[7] investigated the biological responses of renal proximal tubule cells which are exposed to fullerenol, to find that cell death induced by fullerenol is associated with cytoskeleton

disruption. Jin et al.[5] separated fullerenol by two fractions, and they found that the fullerenol fraction with a surface electric charge of -1.913 ± 0.008q ($\times 10^{-6}$ C) could form intermolecular hydrogen bonds with filament at a stoichiometric ratio which could disturb actin filament structure and might inhibit cell locomotion or even induce apoptotic on cells. Besides, the anti-infiltration of tumor and anti-proliferative effect exhibited by fullerenol make it a promising agent with potential antitumor and anticancer.[8-10]

Studies show that cancer progression is related to alterations in cell mechanical properties and responses to mechanical stimuli.[11] The mechanical stability of cells is regulated by dynamic networks of cytoskeletal filaments such as microtubule and actin.[12] Changes in the mechanical phenotype of cells could reveal important information about alternations in cytoskeletal networks, such as changes in the cell rigidity correlated with malignant transformation and cancer progression. In this sense, cyto-mechanical properties could be used as bio-index to distinguish normal cell from its abnormal counterpart. Since fullerenol could inhibit the synthesis of microtubules and disrupt actin filaments,[7, 13] the investigation of cellular mechanical properties subjected to fullerenol treatment would provide instructive information about cancerization.

The last decade witnesses the popularity of cellular elastic modulus being bio-indexed to characterize the biomechanical effects of drug treatment,[14] diseases,[15, 16] and aging.[17] The elastic modulus of individual cells is frequently measured by means of atomic force microscopy (AFM). In the AFM indentation, the load is applied by a cantilever which has been calibrated, and the cantilever tip, either a pyramid, a cone, or a sphere, is brought into contact with the surface of the subject cell. The indentation force and the concurrent indentation depth of tip into the cell are monitored, and the elastic modulus of a single cell can be calculated by fitting the indentation curve with Hertz contact model. However, the Hertz model may ignore the fact that the indentation curve is indeed dependent on the loading rate.[18-20] The determined elastic moduli by means of an elastic contact model might vary with the loading rate and applied load which is inconsistent with the definition of elastic modulus as a material's intrinsic property, which is also very well known as an effect of viscoelasticity of cells[21]. Since it has been confirmed that biological cells exhibit both elastic and viscous behaviors by stress relaxation[22] and creep tests,[23, 24] a more rigorous approach should consider the viscoelastic property of biological cells.

As one of the most important participants in the mechanical integrity of eukaryotic cells, filament actin itself exhibits viscoelastic property[25]. Thus alternations in organization of actin filaments can induce changes not only in their elasticity but also viscosity,[26] which inspires us to use the viscoelastic property as bio-marker to evaluate the effect of cytoskeleton disrupting drugs on cells. In the present study, we implement the quantification and comparison of the viscoelastic properties between the living cancerous cell and its fullerenol-treated counterpart. Hereupon, human hepatocellular carcinoma cells (SMMC-7721) as one of the most common types of cancers worldwide, are presented as subject samples. Both control and treated SMMC-7721 cells are subjected to creep tests realized by AFM indentation[27-29]. The single modal behavior of the cells is analyzed in terms of a *standard solid* model characterized by a single apparent viscosity and two elastic moduli. Taking cell morphology into consideration, we first routinely consider the cells as a spherical shape, and have applied Sneddon's solutions to fit the indentation depth–time curve obtained in the creep test. Then the cell is treated as a thin layer with finite thickness to provide more factual modeling, and a more realistic model, i.e. Dimitriadis model[30] is used to fit the same indentation depth–time curves. We found that both models provided good agreements with

experimental results of indentation depth–time curves. The determination of viscoelastic parameters by the two models confirms the variation in elasticity and viscosity of SMMC-7721 cells induced by fullerenol. The investigation suggests that the quantification of the viscoelastic properties of single living SMMC-7721 cells treated by fullerenol could also be used to evaluate the effect of fullerenol on cancer cells and thus to provide insight into cancer progression.

II. METHODS

A. Cell Preparation

The SMMC-7721 cell line was purchased from the Cell Bank of the Shanghai Institute of Cell Biology, Chinese Academy of Sciences. Cells were cultured in Roswell Park Memorial Institute (RPMI)-1640 medium containing 10% fetal bovine serum (FBS), 100 U/ml penicillin and 100 μg/ml streptomycin, incubated in a humidified atmosphere of 5% CO_2 and at a temperature of 37˚C. After an exponential phase of 24 hour incubation, the cells adhered to the bottom of flask, and they were treated by trypsin so that they could detach the bottom. The detached cells were seeded in a 3.5mm petri dish and incubated for another 24 hours at 37 °C for fullerenol treatment, whereupon cells might undergo morphological changes. The commercial aqueous solution of fullerenol has a concentration of 2 mg/ml, and it was then diluted with RPMI-1640 media with 10% of fetal bovine serum to 0.53 μM/ml. Afterwards, 2 ml of the diluted fullerenol solution was added to the aforementioned petri dish which contained SMMC-7721 cells. For comparison, 2 ml of RPMI-1640 media with 10% of fetal bovine serum was added to the control cells.[31]

B. Atomic Force Microscopy

The module of the AFM employed in this study is JPK NanoWizards 3 BioScience, and it is mounted on an inverted optical microscope, allowing the AFM and optical microscope imaging simultaneously. The criterion for cantilever selection is that the compliance of the cantilever should be around the range of the sample compliance. For very soft and delicate cells, the softest cantilevers are available with spring constants ranging from 0.01 to 0.06 *N/m*.[32] Before indentation, the spring constant of the AFM cantilever was calibrated. A silicon nitride cantilever with the spring constant 0.059 *N/m* after calibration, was used for the cell-tip indentation in this work. The probe is a square pyramid tip with a half-opening angle of β = 25° (half-angle to face), and its radius and height are 10 *nm* and 4 μm respectively. The choice of the probe size is in line with others researchers[33].

FIG. 1

Fig.1(*a*) shows schematically that the displacement of a pyramid tip along a distance δ inwards a half-space material creates a tip-material contact area, which is determined by the contact depth *h*. Since the AFM cantilever tip is a pyramid, the projection area *A* of the tip-sample contact surface is not circular, i.e. not axisymmetric. However, numerical analysis[34, 35] indicates that Fig.1(*a*) could be approximated by the contact between the conic indenter and the substrate material as illustrated in Fig.1(*b*) with a negligible error of 0.012, as long as the conic gives the same projected area-to-depth ratio *A*/*h* as that of the pyramid. In this regard, the half-opening angle β of the conic is 27.75° in order to retain the same area-to-depth ratio of pyramid shown in Fig.1(*a*).

C. Loading details

In order to quantify viscoelastic properties of material of interest, it is a common method to monitor the creep response of material corresponding to an invariant force. To realize the creep test on single cells, the loading history of indentation force is illustrated in Fig.2(*a*). The loading could be approximated by an Heaviside step function as shown in Fig.2(*b*), as long as the ramping period (stage I) is much smaller than the characteristic time constant of the viscoelastic materials.[22] In the present AFM indentation test, the creep tests were achieved by constant force delay mode where the force reaches its maximum value (2 *nN*) within 0.05 seconds and dwells at the peak value for 5 seconds followed by a linear unloading of 40 *nN*/s, as shown in Fig.2(*a*).

D. Theoretical Model

The viscoelastic behavior of materials can be simulated by combinations of elastic elements (springs) and viscous elements (dashpots).[36] The combinations are used to derive equations that describe the deformation of the material subjected to specific loading history. One of the simplest models that predicts creep behavior is called the *standard solid*,[37] which is shown schematically in Fig.2(*c*). It is comprised of an elastic spring, which describes an instantaneous elastic deformation, placed in series with a parallel combination of a spring and dashpot (Kelvin-Voigt element), which describes a delayed elastic deformation.

In the present study, the creep data of the cell are interpreted by the *standard solid* model since we observe evidence for both an instantaneous elastic response and a delayed elastic response. The stress σ applied on the spring element is proportional to its strain ε, i.e. $\sigma = E\varepsilon$, while the stress on the dashpot element is proportional to the rate of its strain, i.e. $\sigma = \eta \cdot d\varepsilon/dt$. The coefficients E and η are the Young's modulus and viscosity respectively. For the constitution shown in Fig.2(*c*), the corresponding constitutive relation is given as

$$\sigma + \frac{\eta}{E_1+E_2}\frac{d\sigma}{dt} = \frac{E_1E_2}{E_1+E_2}\varepsilon + \frac{\eta E_2}{E_1+E_2}\frac{d\varepsilon}{dt} \quad (1)$$

where E_1 and E_2 denote the two spring constants. If the stress σ is a unit Heaviside step function $\sigma = H(t)$, the corresponding output strain is termed as the creep compliance $J(t)$, and it is expressed as

$$J(t) = \frac{1}{E_2} + \frac{1-e^{-t/\tau}}{E_1} \quad (2)$$

where $\tau = \eta/E_1$, termed characteristic retardation time corresponding to the time during which the sample deforms by $1\text{-}e^{-1}$ (or 63.2%) of the total creep deformation. It can be seen from Eq. (2) that $J(0^+) = 1/E_2$, and $J(\infty) = 1/E_1 + 1/E_2$. Thus, the *standard solid* model has an instantaneous modulus $E_0 = E_2$ and equilibrium modulus $E_\infty = E_1E_2/(E_1+E_2)$. It should be born in mind that the three element model is a relatively universal model and it covers two extreme cases. For example, as $E_2 \to \infty$, Fig.2(*c*) degrades to a spring in parallel with a dashpot (Kelvin model) whilst as $E_1 \to 0$, the *three element model* reduces to a spring in series with a dashpot (Maxwell model).

FIG.2

In general, biological cells spread on petri dish in various shapes, some like spheres and some like pancakes.[14, 38, 39] Therefore, we consider cells have either spherical or flattened shapes as

shown in Fig.2(*d*) and (*e*), respectively.

As shown in Fig.2(*d*), if the indentation depth of conic into the cell is small (usually less than one tenth) compared to the height (diameter) of the cell, the cell could be treated as a semi-infinite space. According to the Sneddon's solutions[40] for the elastic deformation of the semi-half substrate under the pressure of a conic indenter, the dependence of indentation depth δ on the indentation force F is given by

$$\delta^2 = \frac{\pi}{2}\frac{(1-\nu^2)cot\beta}{E}F \quad (3)$$

where E and ν denote the Young's modulus and Poisson's ratio of substrate material respectively. For the viscoelastic situation, both Lee and Radok[41] and Ting[42] offered a general solution to linear viscoelastic Boussinesq problem (an infinite half-space indented by an arbitrary shape of rigid axisymmetric and frictionless punch) as long as the contact radius is non-decreasing as the mutual approach increases. According to the theory, substituting the elastic modulus in the Sneddon's solutions with the modulus-displacement convolution in the time domain leads to the relationship between the indentation depth and the applied force as[43]

$$\delta^2(t) = \frac{\pi}{2}cot\beta(1-\nu^2)J(t) * F(t) \quad (4)$$

where β denotes the half-angle of the effective conic as illustrated in Fig.1(*b*), and the asterisk denotes the convolution, i.e.

$$J(t) * F(t) = \int_{\xi=0^-}^{t} J(t-\xi)\frac{d}{d\xi}F(\xi)d\xi \quad (5)$$

Performing Laplace transform on both sides of Eq. (4) yields

$$\mathcal{L}[\delta^2(t)] = \frac{\pi}{2}cot\beta(1-\nu^2)\mathcal{L}[J(t)]\mathcal{L}[\frac{dF(t)}{dt}] \quad (6)$$

Considering that $F(t)$ is a step function, one has

$$\mathcal{L}[\delta^2(t)] = \frac{\pi}{2}cot\beta(1-\nu^2)\mathcal{L}[J(t)]F_{max} \quad (7)$$

Performing inverse Laplace transform on Eq. (7) results in

$$\delta^2 = \frac{(1-\nu^2)\pi cot\beta}{2}J(t)F_{max} \quad (8)$$

where F_{max} denotes the constant load in creep tests. In this study, the cell is assumed as impressible, i.e. ν = 0.5. Thus, fitting Eq. (8) to the δ-t curve obtained by experiment can determine the viscoelastic parameters.

In reality, the SMMC-7721 cells might spread on the petri dish with a finite cell height as shown in Fig.3(*a*) and (*b*), invalidating the semi-infinite assumption of Sneddon's solutions. As can be seen in Fig.3(*c*) and (*d*), the cells have a thickness (H) in the range of several micrometers. Therefore, in this situation, the presence of a stiff substrate may affect transverse deformations,[44, 45] making the sample appearing stiffer than the true value. As a result, it will lead to an overestimation of the measured properties.[46]

FIG. 3

For an elastic substrate material of finite thickness subjected to a conical indenter as shown in

Fig.4, Dimitriadis et al.[30] developed a convenient analytical correction to the Sneddon's solutions due to finite thickness. The dependence of the indentation force F on the indentation depth δ is formulated by[47]

FIG. 4

$$F = \frac{2Etan\beta}{\pi(1-\nu^2)}\delta^2\{1 + 2C(\frac{\delta}{H}) + 16C^2\left(\frac{\delta}{H}\right)^2 + o[\left(\frac{\delta}{H}\right)^3]\} \quad (9)$$

where E, ν, β and H denote the Young's modulus, Poisson's ratio, half-open angle of cone and height of cell respectively. C is a constant given by $C = 1.7795\tan\beta/\pi^2$. It is worth noting that the term outside the brace is identical with Eq. (3), whereas the terms inside the brace are the correction factor due to the finite thickness. If the cell height H tends towards infinitude, the terms inside the brace equal 1, which is exactly the Sneddon's solutions for a semi-infinite substrate. By analogy to the derivation process in Eq. (8), if the substrate material is linear viscoelastic, one has

$$F(t) * J(t) = \frac{2tan\beta}{\pi(1-\nu^2)}\delta(t)^2\{1 + 2C(\frac{\delta(t)}{H}) + 16C^2\left(\frac{\delta(t)}{H}\right)^2 + o[\left(\frac{\delta(t)}{H}\right)^3]\} \quad (10)$$

where J(t) and the asterisk represent the creep compliance and convention respectively. For a creep test, the indentation force is a Heaviside function $F(t) = F_{max}H(t)$. By analogy to the derivation process given by Eq. (4) to (8), one would finally get

$$\delta(t)^2\{1 + 2C(\frac{\delta(t)}{H}) + 16C^2\left(\frac{\delta(t)}{H}\right)^2 + o[\left(\frac{\delta(t)}{H}\right)^3]\} = \frac{\pi}{2}cot\alpha(1-\nu^2)J(t)F_{max} \quad (11)$$

By ignoring the higher order term $o(\cdot)$ in the brace on the left side of Eq. (11), Eq. (11) reduces to a quartic equation whose solution yields the expression of indentation depth $\delta(t)$. Admittedly, the thin layer is not a suitable for the cell morphology. However, within the center cell region, the cell height is relatively even. Since the contact area is smaller compared with this region, we could treat the contact as one between conic and thin film. The creep curves analysis, which includes the viscoelastic curve fitting process, and the parameter extractions were done via MATLAB 2016*b* software.

E. Statistical analysis

Two sample independent *t*-tests were used to determine significant differences between the parameter results of control and treated cells. A 95% confidence interval ($p < 0.05$) was applied to assess the degrees of differences between control and treated cells. All extracted parameters from the AFM based creep data were assessed for significance via statistical tests in GraphPad Prism 7.0 (Graphpad Software Ins., La Jolla, CA).

III. RESULTS AND DISCUSSIONS

The atomic force microscope enables us to monitor the time evolution of the indentation force and the cantilever's concurrent vertical position at all stages. Fig.5(*a*) and (*b*) show the typical input and output of the creep test on living cells respectively. The cantilever's force is kept constant (c.f. Fig.5(*a*)) while the vertical position z of the cantilever varies with time (c.f. Fig.5(*b*)). The force consists of two parts, i.e. the loading part (blue curve) and dwelling part (red curve). In general, the curve of the indentation force should be smooth and flat. However, environmental noises or particles on the media can induce a large deflection of the cantilever, which will be

detected as notch peaks in the output or a drift on the baseline as shown in Fig.5(*a*). In response to the input indentation force shown in Fig.5(*a*), the AFM bead exhibits an approximately linear displacement (see the blue curve in Fig.5(*b*)) and a decay (see the red curve in Fig.5(*b*)), which correspond to the loading and dwelling of indentation force respectively.

FIG.5

Fig.5(*c*) illustrates the schematic of cell and AFM tip at contact (Point *A*) and after puncture (Points *B* and *C*). Owing to the compliance of the AFM cantilever, the vertical displacement of the cantilever bottom (-Δz) does not equal the indentation depth δ after the apex of indenter begins to penetrate the sample cell. The cantilever itself will undergo a deflection Δx as shown in Fig.5(*c*). From geometrical relation, one has

$$-\Delta z = \Delta x + \delta \quad (12)$$

At the same time, the indentation force F will be proportional to the deflection x as

$$F = k\Delta x \quad (13)$$

In the AFM system, both the indentation force F and the displacement of cantilever bottom -Δz are known in advance and therefore the rest unknowns in Eq. (12) and (13) could be derived.

A. Fitting results by using the Sneddon's solutions of pyramid tip on spherical cells

Although the Young's modulus is the frequently adopted parameter to characterize the mechanical properties of biological cells, it does not present a complete description. Fig.6(*a*) and (*b*) show an example of creep deformation for untreated and fullerenol-treated cells respectively, corresponding to the preset force illustrated in Fig.5(*a*). The indentation depth-time curves obtained confirm that the cells undergo a time-dependent deformation in response to a constant loading force, i.e., they creep (Fig.6(*a*) and (*b*)). Therefore, the cells are more-properly described as viscoelastic.

FIG. 6

It can be seen from Fig.6(*a*) and (*b*) that the mechanical response of the cell to the applied force varies on a time scale of several seconds, which is very slow compared with the loading time (see the time interval from point *A* to point *B* in Fig.5). Therefore, the mechanical response of the cell is divided into two components: a fast, elastic response of the cell and a delayed elastic response due to creep deformation.[48] The Sneddon's solutions with *standard solid* model of viscoelasticity theory is used to describe the mechanical response of the cells, which is characterized by three parameters: instantaneous modulus E_0, equilibrium modulus E_∞ and viscosity η, as introduced by Eq. (1) and Fig.2(*c*). Good agreement between the Sneddon's solutions and the creep deformation data could be observed in Fig.6(*a*) and (*b*), with linear correlation coefficient values that are close to one ($R^2 > 0.92$). The average values of the best-fit parameter values obtained for the 100 control and 100 treated cells have been illustrated in Fig.6 (*c*) and (*d*), where one indentation was performed on one subject cell above its nucleus area to alleviate substrate effect as much as possible.[49] Moreover, cytoskeleton structure at this area is more homogeneous and does not show microtubules.[50] We note that the average value of E_0 = 1.74 ± 0.5 kPa and E_∞ = 1.2 ± 0.21 kPa obtained for the control cells, which are significantly higher than their treated counterparts, i.e. E_0

= 1.31 ± 0.29 kPa and E_∞ = 0.99 ± 0.07 kPa. Moreover, it can be seen from Fig.6(*d*) that the average viscosity of control cell η = 682.39 ± 112.7 Pa·s decreases significantly to its treated counterpart η = 402.1 ± 52.4 Pa·s. Based on these extracted parameters, we estimated the characteristic time (η/E_1) of control and treated cells are 0.2s, much longer than the ramping time period (50 ms), and thus the effect of ramping on the identified viscoelastic parameters could be neglected.

Previous studies have already reported that both elasticity and viscosity are heavily impacted by the levels and organization state of actin microfilaments.[25, 26] Jin et al.[5] showed that fullerenol possesses an active structure which could bind actin filaments by enthalpically inducing different morphological features of actin filaments. Owning to this, the binding of cofilin and the severing of actin filaments would be promoted, which forms the cofilin/actin/fullerenol rods. In doing so, the morphology of actin filaments is altered which in turn change the viscoelastic properties of cells. Moreover, by confocal imaging, Liu et al.[33] showed that the morphology of actin filaments transformed from bundles into actin aggregates and finally collapses with time of fullerenol treatment increasing. Since the mechanical properties of biological cells are determined by filaments actin, the disruption of latter induced by fullerenol will deservedly cause the decrease of elastic modulus and viscosity. In sum, the results indicate that remarkable differences in viscoelastic properties between SMMC-7721 cells and their fullerenol treated counterparts, revealing insights into understanding the effect of fullerenol-like anticancer drug in terms of cell mechanics.

B. Fitting results by treating cells as flattened layer

FIG. 7

Fig.7(*a*) and (*b*) present the aforementioned indentation depth–time curves obtained by AFM indentation and the best fitting curves by the Dimitriadis model. The average height of control and treated cells approximate to be 5 and 7 microns respectively measured by AFM deflection imaging. It is suggested that the Dimitriadis model can also fit well the experimental data of the creep test. The fitting results of the determined elastic moduli and viscosity are illustrated in Fig.8(*a*) and (*b*) respectively. It can be seen that both elastic moduli (instantaneous and equilibrium modulus) and viscosity of control cells are higher than that of treated cells, and this tendency is consistent with that predicted by Sneddon's solutions as shown in Fig.6 (*c*) and (*d*).

FIG. 8

For comparison purpose, all the parameters determined by both Sneddon's solutions and Dimitriadis model are plotted in Fig.8(*a*) and (*b*). As can be seen in Fig.8(*a*) and (*b*), each parameter extracted by Dimitriadis model is lower compared to the Sneddon's solutions, which seems inconsistent with the general perception that substrate effect may lead to overestimation of the measured properties. However, it should be noted that the case in the present study is due to finite sample thickness and can be interpreted as follows.[51] During the fitting process in Sect.IIIA and IIIB, we use both Sneddon's solutions (Eq. (8)) and Dimitriadis model (Eq. (11)) to fit the same indentation depth–time curves. If we use J_{Snd}(t) and J_{Dmd}(t) to denote creep compliance

determined by Sneddon's solutions and Dimitriadis model respectively, dividing both sides of Eq. (8) by its homologous sides in 11 yields

$$\frac{1}{1+2C\left(\frac{\delta(t)}{H}\right)+16C^2\left(\frac{\delta(t)}{H}\right)^2} = \frac{J_{snd}(t)}{J_{Dmd}(t)} \quad (14)$$

Since the denominator of right side of Eq. (14) is larger than 1, $J_{Snd}(t)$ is lower than $J_{Dmd}(t)$, i.e. the elastic modulus determined by Sneddon's solutions exceeds that by Dimitriadis model.

C. Rate-jump protocol to determine the intrinsic elastic modulus

Although the standard solid model is assumed, from which elastic modulus and viscosity are quantified, it should be borne in mind the accuracy of the results are dependent on the assumed viscoelastic model which is not easy to verify upfront. In this regard, an appropriate model is desired to allow an effective and intrinsic elastic modulus to be obtained regardless of the particular form of the viscoelasticity model. The rate-jump protocol is a good candidate to accomplish this objective. A full background of the rate-jump protocol is available elsewhere, [27] and will not be repeated here except to present the key parameters and implementation of the analyses. Accordingly, the intrinsic elastic modulus E of the indented cell is given by

$$E = \frac{\Delta\dot{P}(1-\nu^2)}{2a\Delta\dot{d}} \quad (15)$$

where $\Delta\dot{P}$ and $\Delta\dot{d}$ denote the change of the loading rate and displacement rate respectively at the instant of unloading, and a is the corresponding contact area at this moment. According to Sneddon's solution, one has

$$a = \frac{2}{\pi}\delta tan\beta \quad (16)$$

where δ denotes the penetration depth of the conic indenter into the cell at the instant of unloading. One should be aware that $\Delta\dot{d}$ and δ could be determined in Fig.5(b), and $\Delta\dot{P}$ is calculated in Fig.2(a). By using Eq.(15), each δ-t curve will produce one value for the intrinsic elastic modulus, and their average values are compared with the elastic moduli determined by Sneddon's solutions, as illustrated in Fig.8(c). It can be seen that the elastic moduli determined by the rate-jump protocol almost coincide with the instantaneous and equilibrium moduli by Sneddon's solutions regardless of the cell type, and thus the standard solid model would be an appropriate candidate as well to represent the elastic properties of the SMMC-7721 cells.

IV. CONCLUSIONS

In the present study, the fullerenol [$C_{60}(OH)_{24}$]- induced changes in viscoelasticity of living SMMC-7721 cells have been studied by AFM indentation. The SMMC-7721 cell has been modeled at first a semi-infinity and then a flattened layer with finite thickness, and corresponding models have been developed to fit the resulting experimental data. Firstly, the contact area between the pyramid tip and cell is considered as infinitesimal compared to the cell, and the Sneddon's solutions have been used to fit the experimental data of indentation depth–time curves. Secondly, the subject cell is treated as a layer with a finite height, and Dimitriadis model is

utilized to fit the same indentation depth–time curves. The results have shown that both Sneddon's solution and Dimitriadis model can describe very well the behavior of creep tests. Additionally, we have clarified the difference between the extracted parameters by the two models which are fitted to the same indentation depth–time curves, i.e. the difference is due to the correction factor. Moreover, the rate-jump protocol is used to extract the intrinsic elastic modulus of the cell, which almost coincide with the value by Sneddon's solutions, and this indicates that the solid standard model adopted in this study has presented valid estimation in terms of elastic modulus for the SMMC-7721 cells. The determined parameters indicate that not only cell elasticity but also cell viscosity are reduced as a consequence of the fullerenol treatment. It is known that fullerenol could induce actin network which is responsible for cellular mechanical stability, and such physiological modifications to cell will presumably produce corresponding changes to their physical properties, such as their elasticity and viscosity. Therefore the measurement of these properties alternations of SMMC-7721 cells could provide important insights into the mechanism of action of anticancer agents based on fullerenol applications.

ACKNOWLEDGEMENTS

The authors are grateful for the technical supports from the Laboratory of Precision Engineering and Surfaces of the University of Warwick and the International Research Centre for Nano Handling and Manufacturing, Changchun University of Science and Technology. This project has been partially funded by the European Union's Horizon 2020 research and innovation programme under the Marie Skłodowska-Curie grant agreement No 644971 and the China-EU research programme (S2016G4501).

REFERENCES

1. Z. Chen, L. Ma, Y. Liu and C. Chen: Applications of functionalized fullerenes in tumor theranostics. *Theranostics*. **2**, 238 (2012).
2. R. Partha and J.L. Conyers: Biomedical applications of functionalized fullerene-based nanomaterials. *Int J Nanomed*. **4**, 261 (2009).
3. S. Bosi, R.T. Da, G. Spalluto and M. Prato: Fullerene derivatives: an attractive tool for biological applications. *Eur J Med Chem*. **38**, 913 (2003).
4. J. Li, A. Takeuchi, M. Ozawa, X.H. Li, K. Saigo and K. Kitazawa: C-60 Fullerol formation catalyzed by quaternary ammonium hydroxides. *J Chem Soc Chem Commun*. **23**, 1784(1993).
5. J. Jin, Y. Dong, Y. Wang, L. Xia and W. Gu: Fullerenol Nanoparticles with structural activity induce variable intracellular actin filament morphologies. *J Biomed Nanotechnol*. **12**, 1234 (2016).
6. Y.T. Zhou, G.R. Guy and B.C. Low: BNIP-Sa induces cell rounding and apoptosis by displacing p50RhoGAP and facilitating RhoA activation via its unique motifs in the BNIP-2 and Cdc42GAP homology domain. *Oncogene*. **25**, 2393 (2006).
7. D.N. Johnson-Lyles, K. Peifley, S. Lockett, B.W. Neun, M. Hansen, J. Clogston, S.T. Stern and S.E. McNeil: Fullerenol Cytotoxicity in kidney cells is associated with cytoskeleton disruption, autophagic vacuole accumulation, and mitochondrial dysfunction. *Toxicol Appl Pharmacol*. **248**, 249 (2010).
8. J.D. Zhu, Z.Q. Ji, J. W, R.H. Sun, X. Zhang and Y. Gao: Tumor-inhibitory effect and immunomodulatory activity of fullerol $C_{60}(OH)_x$. *Small*. **4**, 1168 (2008).
9. L.H. Lu, Y.T. Lee , H.W. Chen, Y.C. Long and H.C. Huang: The possible mechanisms of the antiproliferative effect of fullerenol, polyhydroxylated C_{60}, on vascular smooth muscle cells. *Brit J Pharmacol*. **123**, 1097 (1998).
10. A.Paraskar, S. Soni, R.A. Mashelkar and S. Sengupta: Fullerenol-cytotoxic conjugates for cancer chemotherapy. *Acs Nano*. **3**, 2505 (2009).
11. S. Iyer, R.M. Gaikwad, V. SubbaRao, C.D. Woodworth and I. Sokolov: Atomic force microscopy detects differences in the surface brush of normal and cancerous cells. *Nat Nanotechnol*. **4**, 389 (2009).
12. T. Hawkins, M. Mirigian, M.S. Yasar and J.L. Ross: Mechanics of microtubules," *J Biomech*. **43**, 23 (2010).
13. J. Mrdanović, S. Solajić, V. Bogdanović, K. Stankov, G. Bogdanovićć and A. Djordjevic, "Effects of fullerenol $C_{60}(OH)_{24}$ on the frequency of micronuclei and chromosome aberrations in CHO-K1 cells," *Mutat Res-Gen Tox En*. **680**, 25 (1999).
14. E. Siamantouras, C.E. Hills, M.Y. Younis, P.E. Squire and K.K. Liu, "Quantitative investigation of calcimimetic R568 on beta cell adhesion and mechanics using AFM single-cell force spectroscopy," *Febs Lett*. **588**, 1178 (2014).

15. G. Thomas, N.A. Burnham, T.A.Camesano and Q. Wen: Measuring the Mechanical Properties of Living Cells Using Atomic Force Microscopy. *J Vis Exp*. **76**, e50497 (2013).
16. C. Rianna and M. Radmacher: Cell mechanics as a marker for diseases: Biomedical applications of AFM. *AIP Conf Proc*. **1760**, 020057 (2016).
17. M.N. Starodubtseva: Mechanical properties of cells and ageing. *Ageing Res Rev*. **10**, 16 (2011).
18. R.E. Mahaffy, S. Park, E. Gerde, J. Käs and C.K. Shih: Quantitative analysis of the viscoelastic properties of thin regions of fibroblasts using atomic force microscopy. *Biophys J*. **86**, 1777 (2004).
19. K.E. Bremmell, A. Evans and C.A. Prestidge: Deformation and nano-rheology of red blood cells: An AFM investigation. *Colloid Surface B*. **50**, 43 (2006).
20. M. Zhao and C. Srinivasan: Rate- and depth-dependent nanomechanical behavior of individual living Chinese hamster ovary cells probed by atomic force microscopy. *J Mater Res*. **21**, 1906 (2006).
21. Q.S. Li, G.Y.H. Lee, C.N. Ong, C.T. Lim: AFM indentation study of breast cancer cells. *Biochem Biophys Res Commun*. **374**, 609 (2008).
22. E.M. Darling, S. Zauscher and F. Guilak: Viscoelastic properties of zonal articular chondrocytes measured by atomic force microscopy. *Osteoarthr Cartilage*. **14**, 571 (2006).
23. E.J. Koay, A.C. Shieh and K.A. Athanasiou: Creep indentation of single cells. *J Biomech Eng*. **125**, 334 (2003).
24. N.D. Leipzig and K.A. Athanasiou: Unconfined creep compression of chondrocytes. *J Biomech*. **38**, 77 (2005).
25. A. Palmer, T.G. Mason, J. Xu, S.C. Kuo and D. Wirtz: Diffusing wave spectroscopy microscopy of actin filament networks. *Biophys J*. **76**, 1063 (1999).
26. A.N. Ketene, P.C. Roberts, A.A. Shea, E.M. Schmelz and M. Agah: Actin filaments play a primary role for structural integrity and viscoelastic response in cells. *Integr Biol (Camb)*. **4**, 540 (2012).
27. A.H.W. Ngan and B. Tang: Response of power-law-viscoelastic and time-dependent materials to rate jumps. *J Mater Res*. **24**, 853 (2009).
28. B. Tang and A.H.W. Ngan: Nanoindentation using an atomic force microscope. *Phil. Mag*. **91**, 1329 (2011).
29. B. Tang and A.H.W. Ngan: Investigation of Viscoelastic Properties of Amorphous Selenium near Glass Transition Using Depth‐Sensing Indentation. *Soft Mater*. **2**, 125 (2004).
30. E.K. Dimitriadis, F. Horkay, J. Maresca, B. Kachar and R.S. Chadwick: Determination of elastic moduli of thin layers of soft material using the atomic force microscope. *Biophys J*. **82**, 2798 (2002).
31. X.Y. Zhu, N. Zhang, Z.B. Wang and X.P. Liu: Investigation of work of adhesion of biological cell (human hepatocellular carcinoma) by AFM nanoindentation. *J Micro-Bio Rob*. **11**, 47 (2016).
32. T. Neumann: JPK Instruments Application Report, 2008.
33. Y. Liu, Z.B. Wang and X.Y. Wang: AFM-Based Study of Fullerenol ($C_{60}(OH)_{24}$)-Induced Changes of Elasticity in Living SMCC-7721 Cells. *J Mech Behav Biomed Mater*. **45**, 65 (2015).
34. R.B. King: Elastic analysis of some punch problems for a layered medium. *Int J Solids Struct*.

23, 1657 (1987).
35. J.M. Antunes, L.F. Menezes and J.V. Fernandes: Three-dimensional numerical simulation of Vickers indentation tests. *Int J Solids Struct*. **43**, 784 (2006).
36. I. M. Ward and D.W. Hadley: *An introduction to the mechanical properties of solid polymers*, 2nd ed. (John Wiley & Sons Ltd, 1993).
37. W.N. Findley, J.S. Lai and K. Onaran: *Creep and relaxation of nonlinear viscoelastic materials with an introduction to linear viscoelasticity*, 3rd ed. (New York: Dover Publications, Inc, 1989).
38. C.E. Hills, M.Y. Younis, J. Bennett, E. Siamantouras, K.K. Liu and P.E. Squires: Calcium-sensing receptor activation increases cell-cell adhesion and *β*-cell function. *Cell Physiol Biochem*. **30**, 575 (2012).
39. J. Chen: Nanobiomechanics of living cells: a review. J *R Soc Interface*. **4**, 20130055 (2014).
40. I.N. Sneddon: The relation between load and penetration in the axisymmetric Boussinesq problem for a punch of arbitrary profile. *Int J Eng Sci*. **3**, 47 (1965).
41. E.H. Lee and J.R.M. Radok: The contact problem for viscoelastic bodies. *J Appl Mech*. **27**, 438 (1960).
42. T.C.T. Ting: The Contact Stresses Between a Rigid Indenter and a Viscoelastic Half-Space. *J Appl Mech*. **33**, 845 (1966).
43. H. L. Yu, Z. Li and Q.J. Wang: Viscoelastic-adhesive contact modeling: Application to the characterization of the viscoelastic behavior of materials. *Mech Mater*. **60**, 55 (2013).
44. J. Chen and G. Lu: Finite element modelling of nanoindentation based methods for mechanical properties of cells. *J Biomech*. **45**, 2810 (2012).
45. J. Chen: Understanding the nanoindentation mechanisms of a microsphere for biomedical applications. *J. Phys. D, Appl. Phys.* **46**, 495303 (2013).
46. J. Sanchez-Adams, R.E. Wilusz and F. Guilak: Atomic force microscopy reveals regional variations in the micromechanical properties of the pericellular and extracellular matrices of the meniscus. *J Orthop Res*. **31**, 1218 (2013).
47. N. Gavara and R.S. Chadwick: Determination of the elastic moduli of thin samples and adherent cells using conical atomic force microscope tips. *Nat Nantechnol*. **7**, 733 (2012).
48. V. Vadillo-Rodriguez, T.J. Beveridge and J.R. Dutcher: Surface viscoelasticity of individual gram-negative bacterial cells measured using atomic force microscopy. *J Bacteriol*. **190**, 4225 (2008).
49. Z.L. Zhou, A.H.W. Ngan, B. Tang and A.X. Wang: Reliable measurement of elastic modulus of cells by nanoindentation in an atomic force microscope. *J Mech Behav Biomed Mater*. **8**, 134 (2012).
50. L. Sirghi, J. Ponti, F. Broggi and F. Rossi: Probing elasticity and adhesion of live cells by atomic force microscopy indentation. *Eur Biophys J*. **37**, 935 (2008).
51. X.Y. Zhu, E. Siamantouras, K.K. Liu and X.P. Liu: Determination of work of adhesion of biological cell under AFM bead indentation. *J Mech Behav Biomed Mater*. **56**, 77 (2015).

Figure Caption

FIG. 1. Schematic of a compliant semi-infinite space indented by (*a*) a square pyramid and (*b*) a conic indenter. α and β denote the half-opening angle of the pyramid and conic indenter respectively, and δ and h represent the indentation depth and the depth beneath the contact periphery respectively.

FIG. 2 Schematic of the AFM indentation force versus time (*a*) and its approximation (*b*) by Heaviside step function. (*c*) Schematic diagram of three element model where a first spring (whose stiffness is E_1) is in parallel with a dashpot and then connected with a second spring (whose stiffness is E_2). The first spring and the dashpot undergo the same deformation, while the force exerted on the second spring equals the sum of forces applied on the first spring and the dashpot. Schematic diagrams of the AFM bead tip in contact with cells of (*d*) spherical shape and (*e*) flattened shape.

FIG. 3. Representative AFM deflection imaging of living SMMC-7721 cells: (*a*) control (*b*) treated cells. (*c*) and (*d*) are the statistical results for control and treated cells respectively.

FIG. 4. Schematic diagram of contact between a rigid conic and a viscoelastic layer with the finite thickness H.

FIG. 5. Schematic diagrams of typical AFM (*a*) force-time and (*b*) displacement-time curve to realize the (*c*) creep test.

FIG. 6. Typical indentation depth–time curves and the best fitting curves by using the Sneddon's solutions for (*a*) control and (*b*) treated cells. The determined (*c*) elastic moduli and (*d*) viscosity by the Sneddon's solutions. The data are presented as average values with standard deviations.

FIG. 7. Typical indentation depth–time curves and the best fitting curves by using the Dimitriadis model for (*a*) control and (*b*) treated cells

FIG. 8. The results of (*a*) elastic modulus and (*b*) viscosity for both control and treated cells determined by the two models in this study. (*c*) The comparison of elastic modulus determined by Sneddon's solutions and that by

rate-jump protocol.

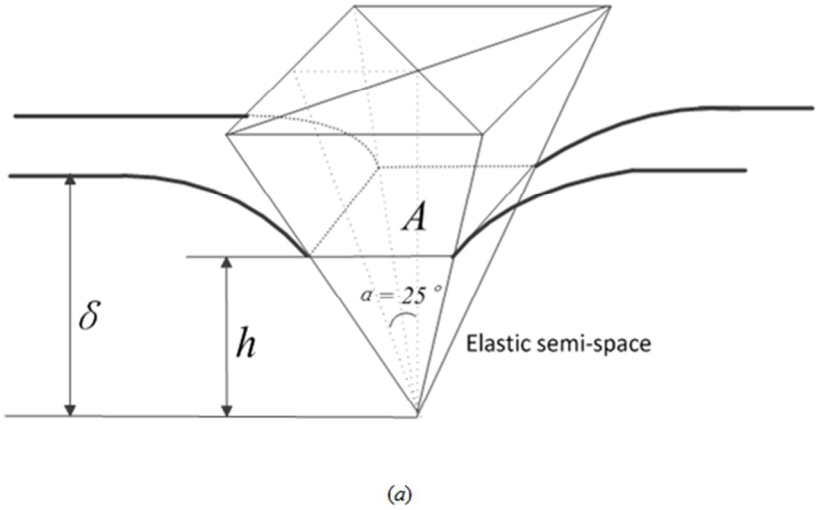

(a)

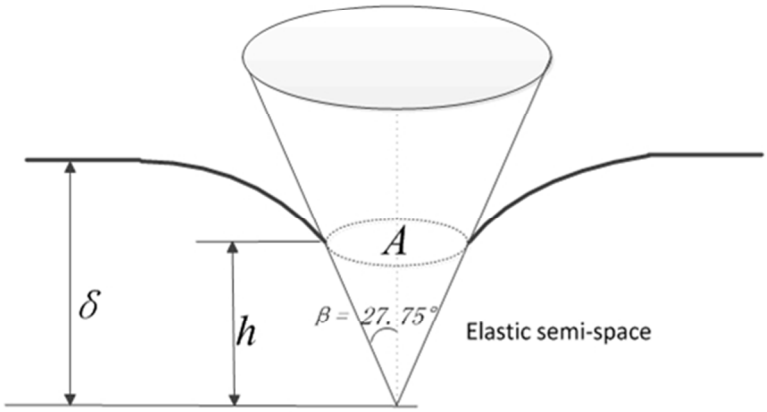

(b)

FIG. 1. Schematic of a compliant semi-infinite space indented by (a) a square pyramid and (b) a conic indenter. α and β denote the half-opening angle of the pyramid and conic indenter respectively, and δ and h represent the indentation depth and the depth beneath the contact periphery respectively.

193x219mm (96 x 96 DPI)

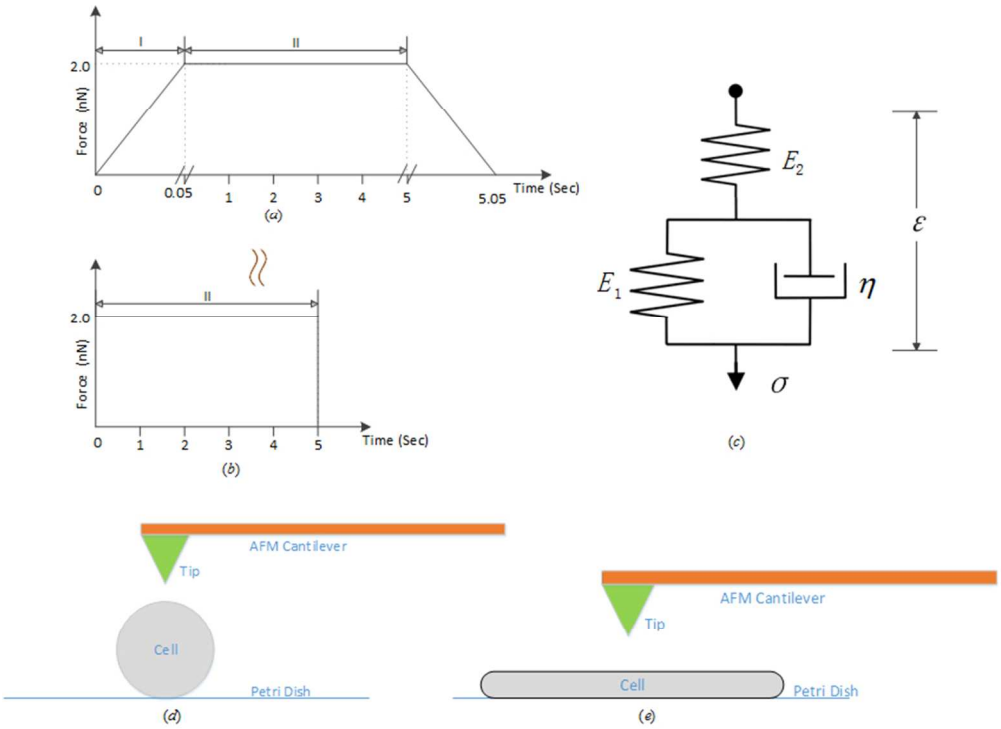

FIG. 2 Schematic of the AFM indentation force versus time (a) and its approximation (b) by Heaviside step function. (c) Schematic diagram of three element model where a first spring (whose stiffness is E1) is in parallel with a dashpot and then connected with a second spring (whose stiffness is E2). The first spring and the dashpot undergo the same deformation, while the force exerted on the second spring equals the sum of forces applied on the first spring and the dashpot. Schematic diagrams of the AFM bead tip in contact with cells of (d) spherical shape and (e) flattened shape.

224x163mm (96 x 96 DPI)

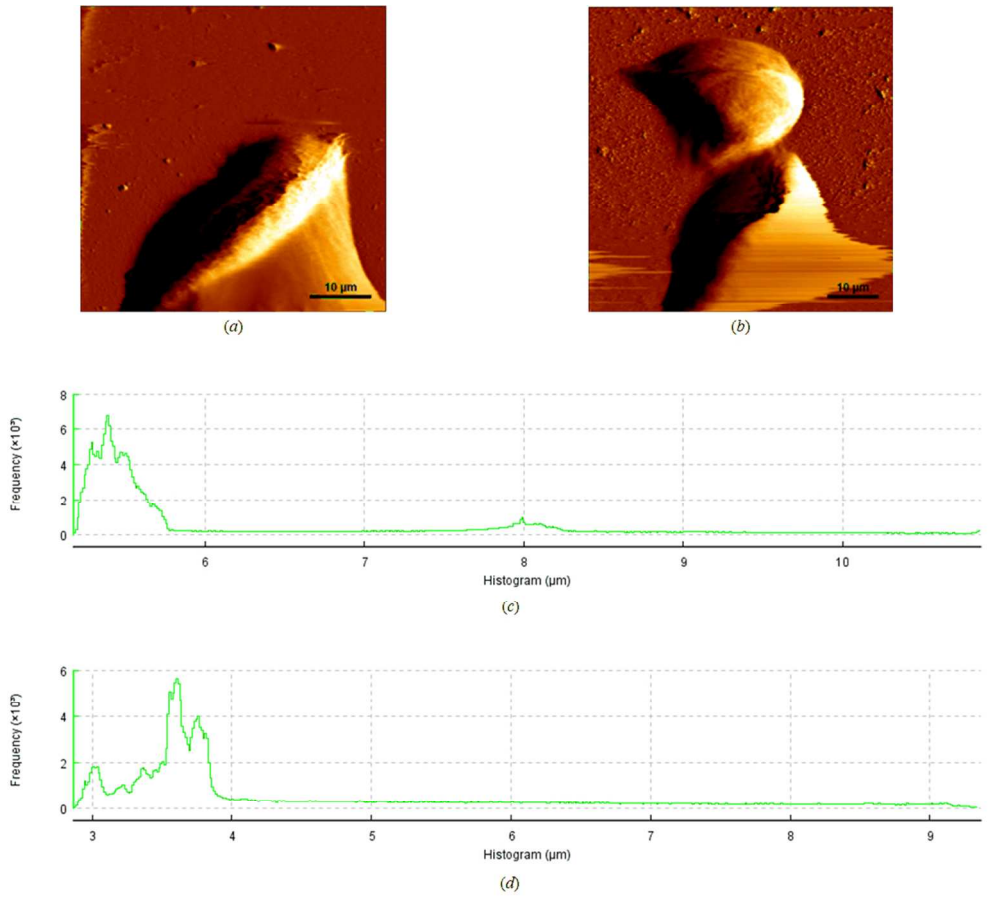

FIG. 3. Representative AFM deflection imaging of living SMMC-7721 cells: (a) control (b) treated cells. (c) and (d) are the statistical results for control and treated cells respectively.

302x270mm (96 x 96 DPI)

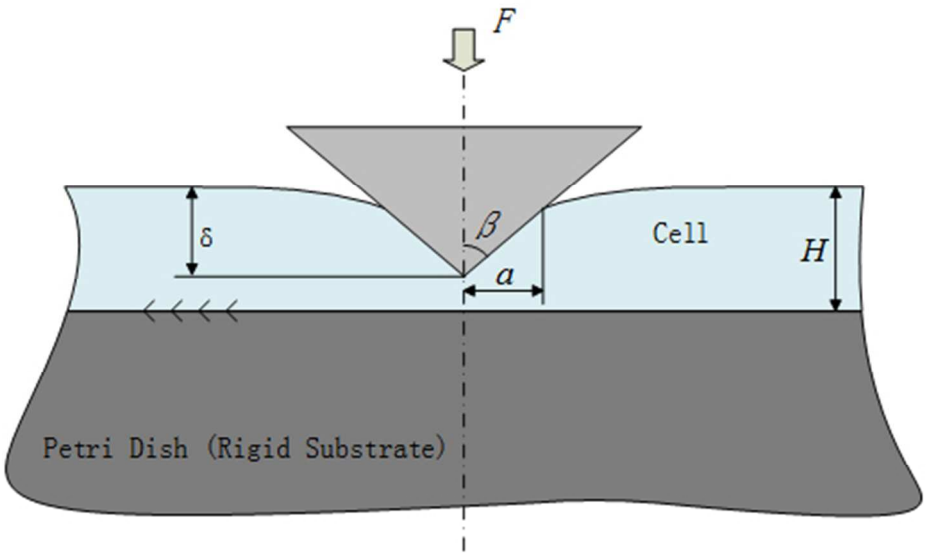

FIG. 4. Schematic diagram of contact between a rigid conic and a viscoelastic layer with the finite thickness H.

144x81mm (96 x 96 DPI)

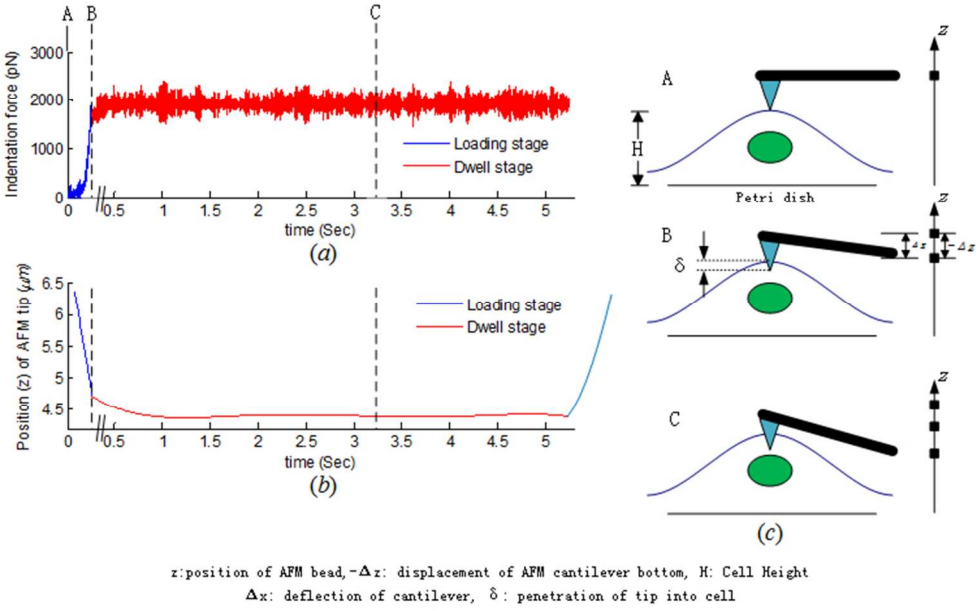

FIG. 5. Schematic diagrams of typical AFM (a) force-time and (b) displacement-time curve to realize the (c) creep test.

203x125mm (96 x 96 DPI)

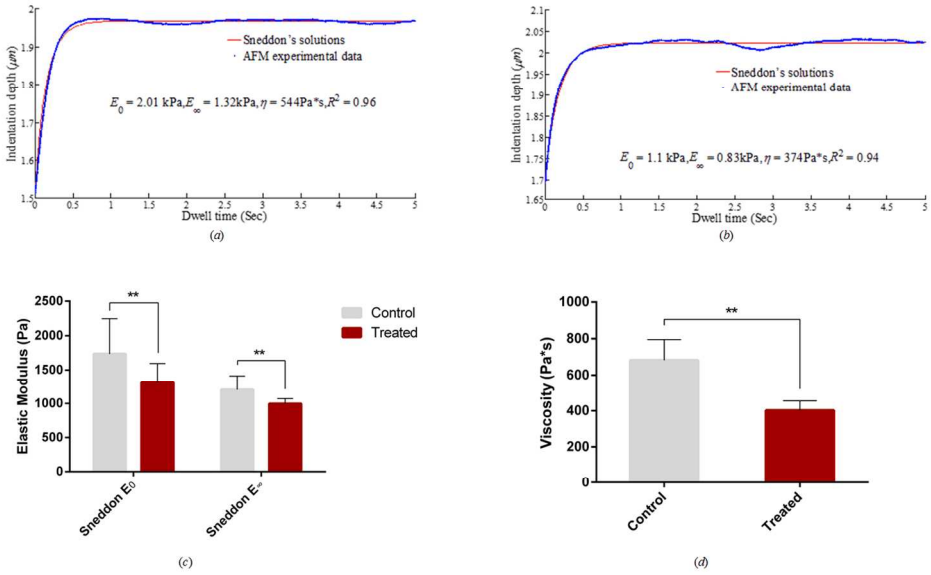

FIG. 6. Typical indentation depth–time curves and the best fitting curves by using the Sneddon's solutions for (a) control and (b) treated cells. The determined (c) elastic moduli and (d) viscosity by the Sneddon's solutions. The data are presented as average values with standard deviations.

397x232mm (96 x 96 DPI)

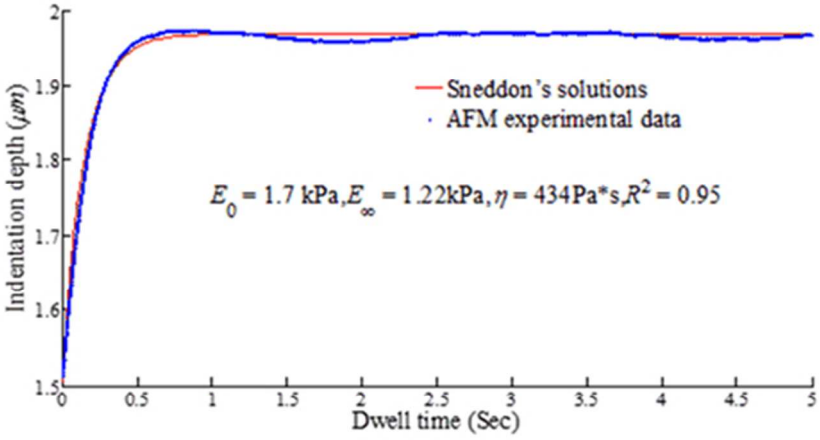

(*a*)

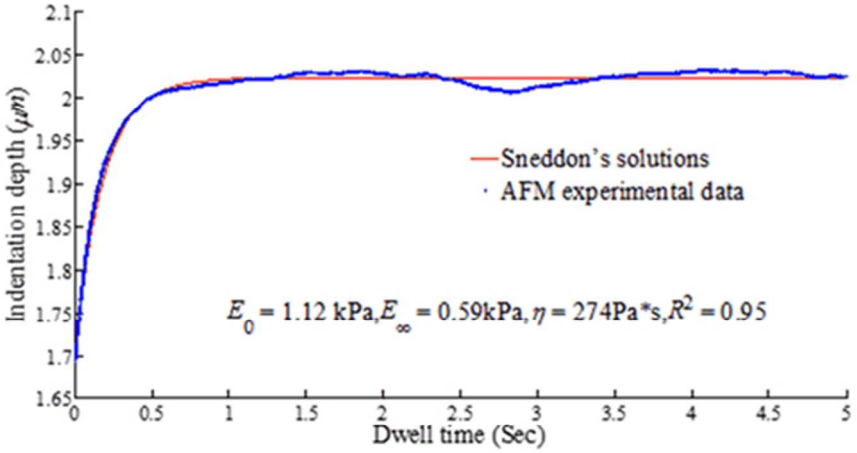

(*b*)

FIG. 7. Typical indentation depth–time curves and the best fitting curves by using the Dimitriadis model for (a) control and (b) treated cells

159x184mm (96 x 96 DPI)

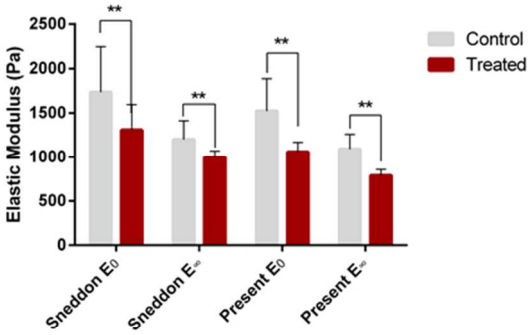

(a)

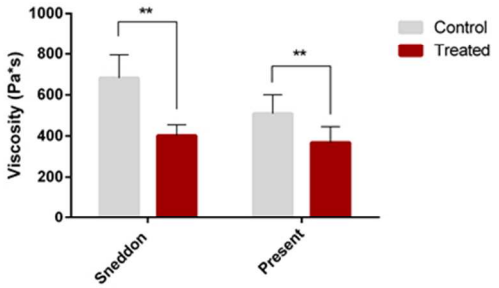

(b)

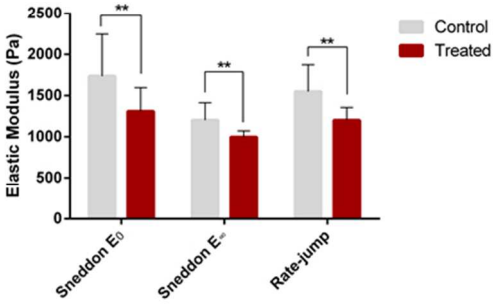

(c)

FIG. 8. The results of (a) elastic modulus and (b) viscosity for both control and treated cells determined by the two models in this study. (c) The comparison of elastic modulus determined by Sneddon's solutions and that by rate-jump protocol.

118x255mm (96 x 96 DPI)